Optics Letters

Critical dimension metrology of a plasmonic photonic crystal based on Mueller matrix ellipsometry and the reduced Rayleigh equation

J.-P. Banon,[1,*] T. Nesse,[1] Z. Ghadyani,[1] M. Kildemo,[1] and I. Simonsen[1,2]

[1]Department of Physics, NTNU Norwegian University of Science and Technology, NO-7491 Trondheim, Norway
[2]Surface du Verre et Interfaces, UMR 125 CNRS/Saint-Gobain, F-93303 Aubervilliers, France
*Corresponding author: jean-philippe.banon@ntnu.no

Received 12 May 2017; revised 31 May 2017; accepted 31 May 2017; posted 31 May 2017 (Doc. ID 295878); published 29 June 2017

A computationally efficient algorithm based on the reduced Rayleigh equation, combined with an optimization scheme, is used to accurately retrieve the morphological parameters of a two-dimensional plasmonic photonic crystal from angle-resolved spectroscopic Mueller matrix ellipsometric measurements. The numerical method is successfully tested against experimental data and gives morphological parameters consistent with SEM and AFM measurements.

OCIS codes: (050.1755) Computational electromagnetic methods; (050.5298) Photonic crystals; (240.2130) Ellipsometry and polarimetry; (290.3200) Inverse scattering.

https://doi.org/10.1364/OL.42.002631

Ellipsometry is a well-established technique for *ex situ* online and offline characterization of homogeneous, inhomogeneous, and nanostructured thin films [1,2]. Indeed, a fast retrieval method allows for extracting in real time the morphological parameters during growth and, hence, reveals the kinetics of the growth processes [3]. Recently, spectroscopic standard, generalized, and Mueller matrix ellipsometry have been suggested for the characterization of surfaces and composite systems of complex geometries, such as photonic crystals and metamaterials [2,4–10].

Spectroscopic ellipsometry has for several decades been used for the characterization of one-dimensional gratings, although limited to non-conical incidence [11,12]. The use of conical incidence was, for example, reported in [13], where the modeling of the Mueller matrix elements was based on the rigorous coupled wave analysis (RCWA), and used to fit the spectroscopic data. Critical dimension retrieval obtained by combining RCWA and Mueller matrix ellipsometry (or scatterometry) has also been investigated for two-dimensional gratings [14,15], and may be regarded as an established, but computationally expensive, technique.

Spectroscopic Mueller matrix ellipsometry of arrays of gold particles supported by a glass substrate was recently shown to exhibit a rich optical response, including Rayleigh–Wood anomalies and significant polarization coupling around the localized surface plasmon resonance (LSPR) [6].

In this Letter, the reduced Rayleigh equation (RRE) [16] is combined with angle-resolved spectroscopic Mueller matrix ellipsometry to produce a computationally efficient and reliable method for the reconstruction of the geometrical parameters of a two-dimensional photonic crystal. The method correctly reproduces the Rayleigh–Wood anomalies and polarization coupling, and is sufficiently fast to practically be used for online metrology. Hence, the proposed method is a promising candidate for fast and accurate inversion of scattering data. Moreover, the RRE method can also be adapted to account for randomness.

We study a two-dimensional photonic crystal made from a rectangular array of oblate hemi-spheroidal gold (Au) particles supported by a fused silica (SiO_2) substrate; see Figs. 1(a)–1(c). The sample was produced by focused ion beam milling of a 40 nm thick Au film. The intention was to produce a square array of particles of a lattice parameter of 210 nm [6,17]. However, SEM and AFM characterization of the sample [Fig. 1(a)] revealed a *rectangular* array of lattice parameters $a_1 = 208 \pm 2$ nm and $a_2 = 211 \pm 2$ nm, where the particles had an in-plane radius of $r_{\parallel} = 58 \pm 4$ nm and a height of $r_{\perp} = 36 \pm 5$ nm [6,17]. This characterization also established that an over-milling into the substrate had taken place during sample preparation which expressed itself as a "trench network" milled into the substrate in regions not covered by Au particles. An accurate estimate of the depth of the trenches was hard to obtain, but a correlation between the SEM and the AFM images supplied the estimate 15 ± 10 nm.

The optical response of the sample was investigated by angle-resolved spectroscopic Mueller matrix ellipsometry in the specular direction. The lower halves of the contour plots in Fig. 1(d) show the experimental results obtained as functions of the azimuthal angle of incidence $\phi_0 \in [0°, 180°]$ and photon energy $\hbar\omega$ for the selected polar angle of incidence $\theta_0 = 55°$. The Mueller matrix elements indicate a rich optical response of the sample, and they show signatures of (1) Rayleigh–Wood anomalies and (2) a LSPR around 2.1 eV [6,17]. The Rayleigh–Wood anomalies appear as a consequence of the periodicity of the sample, and they are due to the opening

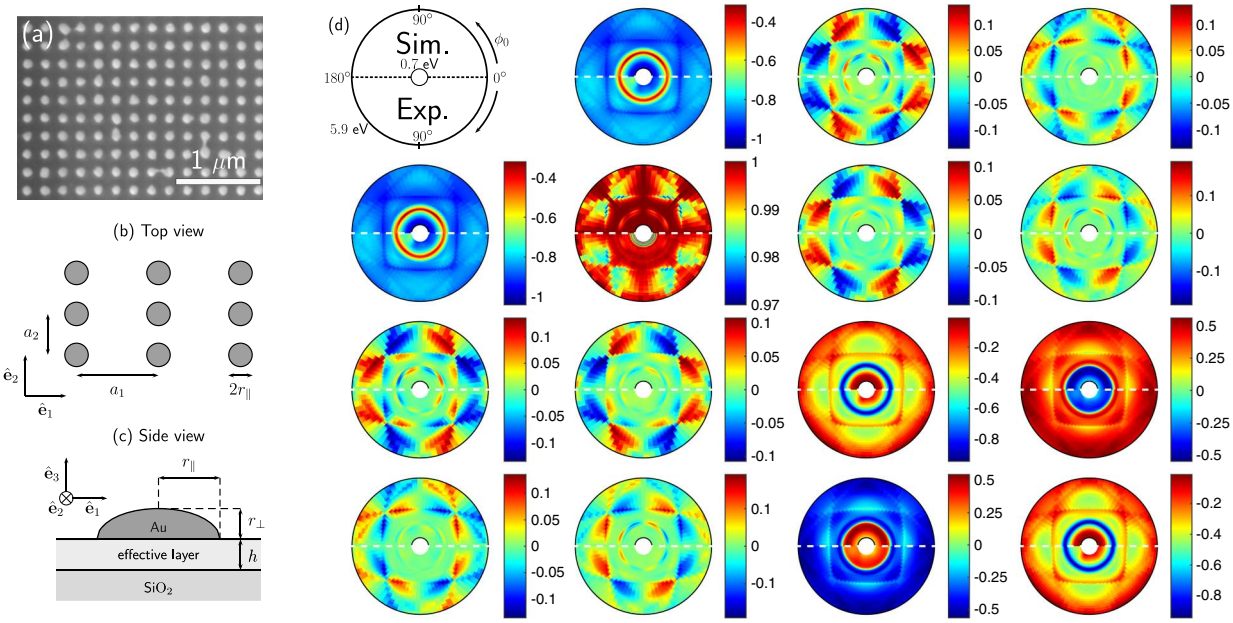

Fig. 1. (a) SEM image of the sample, schematic diagrams of the (b) top and (c) side views of the modeled system. (d) Normalized Mueller matrix elements $m_{ij} = M_{ij}/M_{11}$ $(i,j = 1,\ldots 4)$ as functions of the photon energy $\hbar\omega$ (radial variable) in the range 0.7–5.9 eV and the azimuthal angle of incidence (angular variable) $\phi_0 \in [0°, 180°]$. The lower half of each contour plot represents, for a polar angle of incidence $\theta_0 = 55°$, the experimental m_{ij}-elements measured in the specular direction; the corresponding upper halves present simulation results obtained on the basis of the RRE (1) when assuming the model ELM-opt whose parameters are given in Table 1. Notice from the schematic in the upper-left corner the positive direction assumed for ϕ_0; therefore, a comparison between measured and simulated results should be made symmetrically with respect to the horizontal white dashed lines of each element.

or closing of diffracted channels in reflection or transmission as one scans over the angle of incidence and photon energy (wavelength). A remarkable property of the system under study is the significant polarization coupling observed around the LSPR and the Rayleigh–Wood anomalies, particularly apparent in the off-diagonal blocks of the Mueller matrix.

Fast optical critical dimension metrology based on the recorded Mueller matrix is now demonstrated, uncovering the average morphology of the sample and, hence, producing an optical model further capable of accurately predicting its optical properties at any angle of incidence and scattering. To this end, a theoretical framework for modeling the optical response of the sample is required, and here we will use an approach based on the *RRE* [16,18–21] derived on the basis of the *Rayleigh hypothesis* [22]. In general, this equation is an inhomogeneous, matrix integral equation for the Jones reflection (or transmission) amplitudes. However, under the assumption of a periodic scattering system, the corresponding RRE can be written in the form [20,23] for $\boldsymbol{\ell} \in \mathbb{Z}^2$:

$$\sum_{\mathbf{n}\in\mathbb{Z}^2} \boldsymbol{\mathcal{M}}(\mathbf{p}_{\boldsymbol{\ell}}|\mathbf{p}_{\mathbf{n}})\,\mathbf{R}^{(\mathbf{n})}(\mathbf{p}_0) = -\boldsymbol{\mathcal{N}}(\mathbf{p}_{\boldsymbol{\ell}}|\mathbf{p}_0). \tag{1}$$

Here, $\boldsymbol{\mathcal{M}}(\mathbf{p}_{\boldsymbol{\ell}}|\mathbf{p}_{\mathbf{n}})$ and $\boldsymbol{\mathcal{N}}(\mathbf{p}_{\boldsymbol{\ell}}|\mathbf{p}_0)$ are *known* matrix elements that encode the properties of the scattering system (e.g., the particle shape); explicit expression for these elements can be obtained from Refs. [18,20]. In writing Eq. (1), the projection of the incident wave vector onto the x_1x_2-plane has been denoted:

$$\mathbf{p}_0 = \frac{\omega}{c}\,\sin\theta_0(\cos\phi_0\,\hat{\mathbf{e}}_1 + \sin\phi_0\,\hat{\mathbf{e}}_2), \tag{2}$$

and we have defined $\mathbf{p}_{\mathbf{n}} \equiv \mathbf{p}_0 + \mathbf{G}_{\mathbf{n}}$, where $\mathbf{G}_{\mathbf{n}} = n_1(2\pi/a_1)\hat{\mathbf{e}}_1 + n_2(2\pi/a_2)\hat{\mathbf{e}}_2$ $(n_i \in \mathbb{Z})$ denote the *reciprocal lattice vectors* of the periodic structure. Here, (θ_0, ϕ_0) represents the angles of incidence, ω represents the angular frequency of the incident light, and c represents the speed of light in vacuum. The Jones matrix for reflection into a diffractive order characterized by $\mathbf{n} = (n_1, n_2)$ or, equivalently, a lateral wave vector $\mathbf{p}_{\mathbf{n}}$, is denoted by the 2×2 matrix

$$\mathbf{R}^{(\mathbf{n})}(\mathbf{p}_0) = [R^{(\mathbf{n})}_{\alpha\beta}(\mathbf{p}_0)]_{\alpha,\beta\in\{p,s\}}, \tag{3}$$

where α and β denote the linear polarization states of the reflected and incident light, respectively.

The linear system of equations in Eq. (1) contains an infinite number of unknown reflection amplitudes. A system of finite size is obtained by limiting the $\mathbf{n}$-summation to a set of mode indices such that their corresponding reciprocal lattice vectors lie within a circular domain of radius $G_{\max} = N\,\max(2\pi/a_1, 2\pi/a_2)$ with $N \in \mathbb{N}$, i.e., $|\mathbf{G}_{\mathbf{n}}| \le G_{\max}$ [20,23,24]. In obtaining the numerical results presented in this Letter, the value $N = 15$ was assumed which corresponds to 729 diffractive modes per polarization state of the incident light. The linear system of equations obtained in this way can readily be solved numerically (see Refs. [20,24]) to produce a set of reflection amplitudes $\{\mathbf{R}^{(\mathbf{n})}(\mathbf{p}_0)\}$, from which the elements of the Mueller matrix M_{ij} $(i,j = 1,\ldots,4)$ can be calculated from the formula presented in Ref. [6]. The elements of the normalized Mueller matrix are defined as $m_{ij} = M_{ij}/M_{11}$.

The central processing unit time required to solve Eq. (1) (with $N = 15$) for given angles of incidence and photon energy

was 2.5 s on a desktop computer (Intel i7-5930K 3.5 GHz) when applied to the geometry considered in this Letter. This is significantly shorter, by two orders of magnitude, than the time required to obtain the same result using the commercial FEM package COMSOL. Such a speedup is critical if one wants to do real-time growth monitoring or inversion. Moreover, the memory footprint of the RRE approach is also much smaller than that of COMSOL; we found a memory ratio of 1:60 between the two methods. We must note that the convergence of the numerical solution of the RRE with an increasing number of modes seems not to be guaranteed for energies smaller than 2 eV, which we identified to correspond to a range of energies, where the ratio of the imaginary to the real part of the dielectric constant of gold becomes negatively large and manifests itself with spurious oscillations, as can be seen in Fig. 2. The number of points affected by this issue is small compared with the total number of points used for the optimization problem and, hence, the retrieved parameters are not assumed to be significantly altered.

We now turn to the inversion of the experimental Mueller matrix data from Fig. 1(d) with respect to the morphological parameters characterizing the geometry of the sample. These parameters are the lattice parameters a_1 and a_2; the in-plane radius $r_\parallel$ and the height $r_\perp$ of the gold particles; and, potentially, the thickness h and filling fraction f of a Bruggemann effective medium layer [see Fig. 1(c)] [25]. The determination of these parameters is done in two main steps.

In the first step, the lattice parameters, a_1 and a_2, are determined from the positions of the Rayleigh–Wood anomalies associated with the appearance of diffractive modes of order one in the vacuum region. Theoretically, these Rayleigh–Wood anomalies (in reflection) are expected at values of $(\phi_0, \hbar\omega)$ for which $|\mathbf{p}_{\boldsymbol{\ell}}| = \omega/c$ [6]; this condition contains the two lattice parameters, but is *independent* of the other morphological parameters. From the experimental Mueller matrix elements, the positions of the Rayleigh–Wood anomalies are extracted as functions of the azimuthal angle of incidence ϕ_0 and photon energy $\hbar\omega$ (see Ref. [6] for details), and the theoretical prediction for the corresponding modes are fitted to the resulting data. In this way, using the Rayleigh–Wood anomalies associated with the modes $\boldsymbol{\ell} = (-1, 0)$ and $\boldsymbol{\ell} = (0, -1)$, it was determined that $a_1 = 205.6 \pm 2.0$ nm and $a_2 = 210.9 \pm 2.0$ nm. Here, the error bars are estimated from how accurately the positions of the anomalies can be extracted from the experimental data. The obtained values for the lattice parameters are in good agreement with those measured by SEM and AFM.

In the second step of the inversion, the lattice parameters are held fixed at the values obtained during the first step, while the remaining parameters, or a subset of them, $\mathbf{v} \subseteq \{r_\parallel, r_\perp, h, f\}$, are determined by fitting the output of the theoretical model (1) to the corresponding measured data. To this end, we defined the cost or objective function as

$$\chi^2(\mathbf{v}) = \frac{1}{2}\sum_{\mathbf{p}_0,\omega}\sum_{i,j}[m_{ij}(\mathbf{p}_0,\omega|\mathbf{v}) - \tilde{m}_{ij}(\mathbf{p}_0,\omega)]^2. \quad (4)$$

Here, $m_{ij}(\mathbf{p}_0, \omega|\mathbf{v})$ denotes an element of the normalized Mueller matrix obtained from the model for a *given* set of morphological parameters $\mathbf{v}$, which depends on the lateral wave vector of incidence $\mathbf{p}_0$ [or angles (θ_0, ϕ_0), Eq. (2)] and the photon energy $\hbar\omega$; the corresponding measured normalized Mueller matrix element is denoted $\tilde{m}_{ij}(\mathbf{p}_0, \omega)$. The outer sum that appears in Eq. (4) was performed over a set of 1501 values in the $(\phi_0, \hbar\omega)$-plane, since $|\mathbf{p}_0|$ (or θ_0) was assumed constant in the experiment. This set was constructed by selecting 19 values for the azimuthal angle of incidence $\phi_0 \in [0°, 90°]$ with a step of 5°; and 79 photon energies were chosen uniformly between 1.5 and 5.9 eV. In the definition of $\chi^2(\mathbf{v})$, only the elements $(i, j) \in \{(1, 2), (3, 3), (3, 4)\}$ were taken into account in the inner sum of Eq. (4) in the sets of block-diagonal Mueller matrix elements related by symmetries [26]. Note that off-block diagonal elements were not included.

The first set of inversion results was obtained under the assumption that the Au hemi-spheroids were supported by a *planar* SiO_2 substrate. The parameters that one intends to retrieve, therefore, are $\mathbf{v} = (r_\parallel, r_\perp)$. The minimization of the cost function $\chi^2(\mathbf{v})$, for this and later models, was performed using the Levenberg–Marquardt algorithm where the Jacobian was calculated by a finite-difference approach [27]. The dielectric functions were obtained from oscillator fits to multiple data sets of SiO_2 [28] and the inversion of ellipsometric measurements on the 40 nm thick uniform Au film performed prior to milling. In this way, the reconstruction gave the values $r_\parallel = 59.7$ nm and $r_\perp = 39.9$ nm [Table 1, row labeled Au/SiO_2]. The photon energy dependence of the resulting Mueller matrix elements that contributes to $\chi^2(\mathbf{v})$ is presented as the dotted lines in Fig. 2(a) for $\phi_0 = 0°$, and they show good agreement with the corresponding measured data [solid lines]. It is observed that the energy of the LSPR at 2.1 eV is well reproduced by the Au/SiO_2 model. The same is true for the location of the Rayleigh–Wood anomalies, consistent with the proposed approach for the determination of the lattice parameters a_i. Figure 2(b) depicts the energy dependence of the

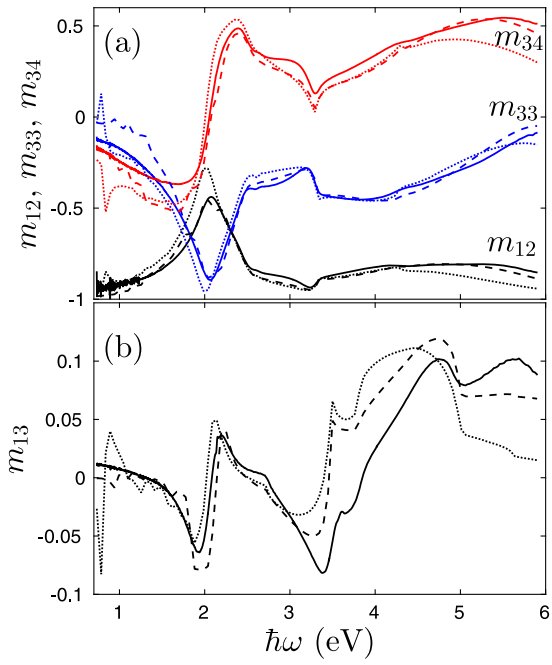

Fig. 2. Mueller matrix elements (a) m_{12}, m_{33}, and m_{34} for $\phi_0 = 0°$ and (b) m_{13} for $\phi_0 = 20°$ as functions of photon energy. The different lines correspond to the experimental data (solid lines); the Au/SiO_2-model (dotted lines) and ELM-opt (dashed lines). The parameters assumed in the modeling are given in Table 1, and the polar angle of incidence was $\theta_0 = 55°$.

Table 1. Microscopy and Reconstructed Morphological Parameters for the Different Models for Lattice Parameters $a_1 = 205.6$ nm and $a_2 = 210.9$ nm[a]

Model	$r_\parallel$ (nm)	$r_\perp$ (nm)	h (nm)	f	χ^2
SEM, AFM	58 ± 4	36 ± 5	15 ± 10	—	—
Au/SiO_2	59.7	39.9	—	—	18.9
ELM-10	59.3	38.7	**10**	0.540	12.4
ELM-20	59.9	37.4	**20**	0.458	9.0
ELM-opt	59.6	36.7	33.5	0.517	6.4

[a]Parameters in bold were kept constant during optimization.

off-block diagonal element m_{13} for $\phi_0 = 20°$. Although this element was not used in the optimization, a qualitatively good agreement is found between the experiment and the Au/SiO_2 model. Similar results were observed for the other Mueller matrix elements and/or other values of ϕ_0 and θ_0 (results not shown).

From the results presented in Fig. 2, it is observed that the agreement between the measured and the Au/SiO_2 model results are best in the low energy region. We speculate that the poorer agreement observed for high energies is mainly due to the non-planar features of the surface of the substrate that is caused by overmilling. A simple effective layer characterized by its thickness h and filling fraction f between air and glass was used to model the overmilling into the glass. We considered three such effective layer models (ELMs) corresponding to the fixed thickness $h = 10$ nm, 20 nm, and $\mathbf{v} = (r_\parallel, r_\perp, f)$, or variable thickness and $\mathbf{v} = (r_\parallel, r_\perp, h, f)$. Optimization performed on the basis of these models resulted in the morphological parameters presented in Table 1. Of the three considered models, ELM-opt represents best measured data in terms of the lowest value for χ^2. As the thickness of the effective layer is increased to 33.5 nm, the value of $r_\parallel$ remains stable, and the value of $r_\perp$ decreases, while the filling fraction f is rather stable. Figure 2 presents as dashed lines the energy dependence of some of the m_{ij}-elements that were obtained from ELM-opt when assuming parameters in Table 1. It is apparent from the results of this figure that the ELM-opt better represents the measured data than the Au/SiO_2 model; in particular, this is the case in the high energy region.

Figure 1(d) presents the full $(\phi_0, \hbar\omega)$ dependence of all normalized Mueller matrix elements obtained from (1) the reduced Rayleigh Eq. (1) (upper halves of the contour plots) and (2) the measurements. The morphological parameters assumed in obtaining the simulation results were those of ELM-opt (see Table 1). The results of Fig. 1(d) show good agreement between *all* the measured and modeled Mueller matrix elements, and not only those used in the minimization. It is noted that similar results to those presented in Fig. 1(d) were obtained within the Au/SiO_2 model, except for larger discrepancies between measured and modeled data at high energies.

In conclusion, we have presented a method that combines the RRE with angle-resolved spectroscopic Mueller matrix ellipsometry, giving a computationally efficient and reliable approach for the reconstruction of the morphological parameters of a two-dimensional plasmonic photonic crystal. The approach is successfully applied to experimental Mueller matrix ellipsometry data, and the reconstructed morphological parameters are found to be consistent with microscopy measurements. The RRE approach can readily be generalized to multilayer systems, and/or quasi-random systems. The proposed method can be adapted to engineering of systems with well-defined optical properties. Moreover, it has the potential of being used for automatic large scale optical characterization, quality assessment, and monitoring applications. Furthermore, the morphological parameters extracted from Mueller matrix measurements performed in the specular direction for a limited number of angles of incidence, in combination with the RRE, can be used to predict the optical response at any angles of incidence and scattering. Such possibilities will be the topic of future studies.

Funding. Norges Forskningsråd (213453, 216699); Agence Nationale de la Recherche (ANR) (ANR-15-CHIN-0003).

REFERENCES

1. H. G. Tompkins and E. A. Irene, *Handbook of Ellipsometry* (William Andrew, 2005).
2. M. Losurdo and K. Hingerl, *Ellipsometry at the Nanoscale* (Springer, 2012).
3. I. S. Nerbø, S. L. Roy, M. Foldyna, E. Søndergård, and M. Kildemo, Opt. Express **19**, 12551 (2011).
4. T. Oates, H. Wormeester, and H. Arwin, Prog. Surf. Sci. **86**, 328 (2011).
5. T. Oates, Appl. Surf. Sci. **258**, 9278 (2012).
6. T. Brakstad, M. Kildemo, Z. Ghadyani, and I. Simonsen, Opt. Express **23**, 22800 (2015).
7. V. G. Kravets, F. Schedin, and A. N. Grigorenko, Phys. Rev. Lett. **101**, 087403 (2008).
8. V. G. Kravets, F. Schedin, G. Pisano, B. Thackray, P. A. Thomas, and A. N. Grigorenko, Phys. Rev. B **90**, 125445 (2014).
9. B. Gompf, J. Braun, T. Weiss, H. Giessen, M. Dressel, and U. Hübner, Phys. Rev. Lett. **106**, 185501 (2011).
10. A. Berrier, B. Gompf, L. Fu, T. Weiss, and H. Schweizer, Phys. Rev. B **89**, 195434 (2014).
11. B. K. Minhas, S. A. Coulombe, S. Sohail, H. Naqvi, and J. R. McNeil, Appl. Opt. **37**, 5112 (1998).
12. X.-T. Huang and F. L. Terry, Jr., Thin Solid Films **468**, 339 (2004).
13. T. Novikova, A. De Martino, S. Ben Hatit, and B. Drévillon, Appl. Opt. **45**, 3688 (2006).
14. B. Kaplan, T. Novikova, A. De Martino, and B. Drévillon, Appl. Opt. **43**, 1233 (2004).
15. M. Foldyna, A. De Martino, E. Garcia-Caurel, R. Ossikovski, C. Licitra, F. Bertin, K. Postava, and B. Drévillon, Eur. Phys. J. **42**, 351 (2008).
16. I. Simonsen, Eur. Phys. J. **181**, 1 (2010).
17. M. Kildemo, J.-P. Banon, A. Baron, T. Brakstad, and I. Simonsen, Appl. Surf. Sci. (2017, to appear).
18. A. Soubret, G. Berginc, and C. Bourrely, Phys. Rev. B **63**, 245411 (2001).
19. A. Soubret, G. Berginc, and C. Bourrely, J. Opt. Soc. Am. A **18**, 2778 (2001).
20. M. Kretschmann and A. A. Maradudin, Phys. Rev. B **66**, 245408 (2002).
21. T. Nordam, P. Letnes, and I. Simonsen, Front. Phys. **1**, 8 (2013).
22. A. G. Voronovich, *Light Scattering and Nanoscale Surface Roughness*, A. A. Maradudin, ed. (Springer, 2006), Chap. 4, pp. 93–104.
23. T. Nordam, P. Letnes, I. Simonsen, and A. A. Maradudin, Opt. Express **20**, 11336 (2012).
24. J.-P. Banon, M. Kildemo, and I. Simonsen (unpublished).
25. V. A. Markel, J. Opt. Soc. Am. A **33**, 1244 (2016).
26. A. Schönhofer and H.-G. Kuball, Chem. Phys. **115**, 159 (1987).
27. W. H. Press, S. A. Teukolsky, W. T. Vetterling, and B. P. Flannery, *Numerical Recipes: The Art of Scientific Computing*, 3rd ed. (Cambridge University Press, 2007).
28. C. M. Herzinger, B. Johs, W. A. McGahan, J. A. Woollam, and W. Paulson, J. Appl. Phys. **83**, 3323 (1998).